Does Förster Theory Predict the Rate of Electronic Energy Transfer for a Model Dyad at Low Temperature?

Carles Curutchet,*,† Benedetta Mennucci,‡ Gregory D. Scholes,§ and David Beljonne||

Dipartimento di Chimica Generale ed Inorganica, Chimica Analitica e Chimica Fisica, Università di Parma, Parco Area delle Scienze, I-43100 Parma, Italy, Dipartimento di Chimica e Chimica Industriale, Università di Pisa, via Risorgimento 35, 56126 Pisa, Italy, Department of Chemistry, 80 St. George Street, Institute for Optical Sciences, and Centre for Quantum Information and Quantum Control, University of Toronto, Toronto, Ontario M5S 3H6 Canada, and Laboratory for Chemistry of Novel Materials, University of Mons-Hainaut, Place du Parc 20, B-7000 Mons, Belgium

Received: November 6, 2007; In Final Form: January 4, 2008

The use of the Förster model to predict the dynamics of resonant electronic energy transfer (RET) in a model donor−acceptor dyad (a terphenyl-bridged perylene diimide (PDI)−terrylene diimide (TDI) dyad molecule) embedded at low temperature in a PMMA matrix is tested against experiment. The relevant ingredients involved in the Förster rate for RET, namely electronic coupling, spectral overlap, and screening effects, are accounted for in a quantitative manner. Electronic couplings are obtained from time-dependent density functional theory calculations, and the effect of the PMMA environment is included both on the transition densities and on their interaction through the IEFPCM model. We find that the presence of the terphenyl bridge induces a slight delocalization of the PDI and TDI transition densities over the bridge originating in a 56% increase in the coupling and in the breakdown of the dipole−dipole approximation. The spectral overlap is determined on the basis of a detailed simulation of the homogeneously broadened donor emission and acceptor absorption line shapes determined by fitting the single molecule spectra measured at 1.2 K. The corresponding distribution of spectral overlap throughout the ensemble is then estimated by assuming an uncorrelated inhomogeneous line broadening for the donor and acceptor. Combining the calculated electronic couplings and spectral overlaps sampled from Monte Carlo realizations of the energetic disorder, we obtain a mean RET time (∼8 ps) and a distribution in reasonable agreement with experiment.

1. Introduction

Resonant electronic energy transfer (RET) involves a virtual photon exchange between two molecules and is a ubiquitous process in materials and life science.[1] RET is for instance used to harvest light in photosynthesis[2−4] or as a spectroscopic ruler for the measurement of distances in proteins.[5−7] The powerful machinery designed by nature through evolution has inspired scientists to take advantage of fast and directional energy transfer processes in the development of synthetic light harvesting systems. Namely, one can take advantage of RET to achieve high internal quantum efficiencies in organic-based light emitting diodes,[8−10] to drive the electronic excitations toward charge-separation interfaces in photovoltaic cells[11−13] or to promote delicate (bio)chemical sensing.[14−21]

In recent years much attention has been devoted to the modeling of electronic energy transfer in complex assemblies of molecules.[22,23] In this context, Förster theory[24] has been successfully applied to describe the dynamics of RET in the case of dipole allowed electronic transitions. One of the key features of the Förster model is that the rate for energy transfer can be cast into simple spectroscopic observables including absorption coefficient and emission line shape and quantum yield. The derivation of the Förster equation rests on the golden rule (GR) and the weak coupling approximation, according to which the electronic interaction between the molecules is small in comparison to the coupling to the bath. In the time domain, this translates into a fast thermalization on the donor prior to the slower energy hopping event from the donor to the acceptor. In addition to the main limitations inherent to the weak coupling regime (i.e., hot transfer and/or memory effects are neglected), the Förster model implies additional approximations in the calculation of the two important ingredients involved in the GR formulation of the energy transfer rate (see below): the electronic coupling and the spectral overlap factors. Namely, the Förster rates are obtained: (i) after averaging away the shape of the excited-state wavefunctions onto simple point dipoles that interact through space in a dielectric continuum; and (ii) on the basis of donor and acceptor spectral lineshapes measured at the ensemble level. A more rigorous treatment requires: (i) calculating the coupling from transition densities not limited to a point dipole description[1,25−32] and accounting for distance-dependent dielectric screening effects;[33,34] and (ii) estimating the spectral overlap from the single molecule homogeneously broadened absorption and emission spectra and subsequently averaging over inhomogeneous, i.e., static, disorder to simulate the ensemble data.[35,36]

Recent single molecule spectroscopy (SMS) experiments have pointed to a breakdown of the Förster model in model dyad and triad conjugated structures.[37−39] Namely, an efficient intramolecular energy transfer was reported by Becker et al. in

* To whom correspondence should be addressed. E-mail: carles@dcci.unipi.it.
† Università di Parma.
‡ Università di Pisa.
§ University of Toronto.
|| University of Mons-Hainaut.

10.1021/jp7106507 CCC: $40.75
Published on Web 03/05/2008

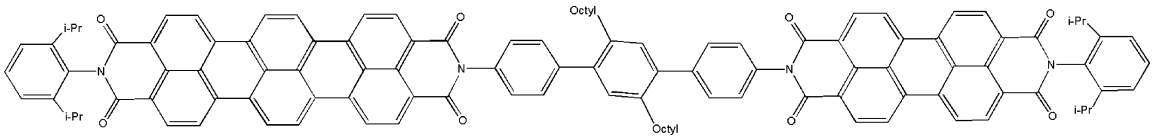

Figure 1. Structure of the PDI−TDI dyad studied in this work.

single chains of polyindenofluorene end-capped with perylene monoimide moieties in absence of spectral overlap.[37,38] The significant red shift of the dye absorption spectrum when grafted to the polymer backbone suggests strong coupling possibly mediated by through-bridge interactions between the end-caps and the polyindenofluorene, which could potentially explain the non-Förster behavior in this case. More surprising is another set of low-temperature SMS data showing a departure from the relationship between energy transfer rates and spectral overlaps in the case of perylene diimide (PDI)−terrylene diimide (TDI) dyads bridged by a substituted terphenyl spacer.[39] There, the absorption spectra of the donor (PDI) and acceptor (TDI) units essentially superimpose to that of the dyad suggesting weak electronic coupling. In this work, we address the efficiency for the energy transfer rate in these dyads with the emphasis on the role of the bridge and the polarizable medium on the electronic couplings and on the basis of a careful simulation of the spectral lineshapes.

2. Methods

2a. Electronic Energy Transfer. The rate of RET between molecules or donor and acceptor chromophores in a supermolecular system is dependent on the interchromophore separation, their relative orientation, the strengths of the transition dipole moments (i.e., electronic coupling, *V*), and spectral overlap, *J*, between donor emission and acceptor absorption.[1] According to the weak coupling, Markovian, limit, the RET rate *k* is given by

$$k = \frac{2\pi}{\hbar}|sV_s|^2 J \tag{1}$$

where V_s is the electronic coupling including the implicit solvent effect, while *s* is the factor accounting for screening of the Coulombic interactions between donor and acceptor by the medium:[33,34] the explicit solvent screening that is taken to be $1/n^2$ in Förster theory. We use *ab initio* quantum-chemical methods accounting for solvent effects to evaluate the Coulombic interaction between donor and acceptor transition densities, as described below. *J* is the spectral overlap obtained from the integrated area between area normalized donor emission and acceptor absorption line shapes that we determine based on experimental data.

In the present work we examine the application of eq 1 for the prediction of the RET rate in a model dyad. It is of current interest to know where this equation may be limited, particularly with respect to its application for low-temperature studies. We focus particularly on estimating accurately the principle ingredients in eq 1: electronic coupling, spectral overlap, and solvent screening. For example, we address questions such as: Is the point dipole approximation valid? What are the contributions from superexchange (through-bridge) interactions? How does ensemble averaging distort the spectral overlap? What is the magnitude of the solvent screening?

2b. Electronic Coupling Calculations. Electronic couplings were obtained from time-dependent density functional theory (TD−DFT) calculations in which the effect of the surrounding environment was introduced through the *integral equation formalism* (IEF)[40] version of the polarizable continuum model (PCM).[41] In the PCM model, the system under scrutiny (the "solute") is fully described at a quantum-mechanical level, while the surrounding environment (the "solvent") is described as a polarizable continuum characterized by its macroscopic dielectric properties. The polarization response of the solvent is then described as a set of *apparent surface charges* (ASC) displaced on an appropriately molecular-shaped cavity surface, which represents the solute−solvent boundary (see ref 42 for an exhaustive review). In this framework, electronic couplings were obtained from a perturbative approach as the interaction between the transition densities of the non-interacting chromophores, where PCM solvent effects are accounted for self-consistently, both on the transition densities themselves and on their interaction.[29,43] To first-order, the electronic coupling, *V*, writes:

$$V = V_s + V_{\text{explicit}} \tag{2a}$$

$$V_s = \int d\mathbf{r} \int d\mathbf{r}'\, \rho_A^{T*}(\mathbf{r}')\left(\frac{1}{|\mathbf{r}'-\mathbf{r}|} + g_{xc}(\mathbf{r}',\mathbf{r})\right)\rho_D^T(\mathbf{r}) - \omega_{D/A}\int d\mathbf{r}\rho_A^{T*}(\mathbf{r})\rho_D^T(\mathbf{r}) \tag{2b}$$

$$V_{\text{explicit}} = \sum_k \left(\int d\mathbf{r}\rho_A^{T*}(\mathbf{r})\frac{1}{|\mathbf{r}-\mathbf{s}_k|}\right) q(s_k;\epsilon_\omega,\rho_D^T) \tag{2c}$$

where $\rho_{D/A}^T$ ($\omega_{D/A}$) indicate transition densities (energies) of the solvated donor (D) and acceptor (A), respectively, in the absence of their interaction; $g_{xc}(\mathbf{r}',\mathbf{r})$ is the exchange plus correlation kernel; *q* are the ASCs located at the center s_k of the discrete surface elements in which the cavity surface is partitioned; *r* is the electronic coordinate; and ϵ_ω is the frequency-dependent dielectric permittivity of the medium. In the RET process, ϵ_ω will approximately coincide with the optical permittivity ϵ_{opt}, i.e., the square of the refractive index *n*.

In eq 2b, V_s describes a chromophore−chromophore Coulomb and exchange-correlation interaction (through the kernel g_{xc}) corrected by an overlap contribution. As the values of the transition densities can be significantly modified by the reaction field produced by the polarized medium, then V_s term carries an *implicit* solvent effect. In addition, the solvent explicitly enters into the definition of the coupling through the term in eq 2c, V_{explicit}, which describes an indirect interaction between the two chromophores mediated by the medium. This latter term generally leads to an overall reduction (i.e., screening) of the D/A coupling. Within this framework, the solvent screening factor entering eq 1 is defined as $s = V/V_s = (V_s + V_{\text{explicit}})/V_s$.

Initially, geometry optimization at the B3LYP/6-31G(d) level was carried out in the gas phase for the complete PDI−TDI dyad (see Figure 1), as very small changes in the geometries are expected to arise upon solvation. Basché and co-workers have shown that there is a slight change in geometry when the dyad is embedded in a PMMA matrix,[44] namely an average deviation of 20° from the linear conformation which was

attributed to the flexibility of the *p*-phenylene spacer. Such a distortion has not been taken into account in the present study but its final effect is expected to be small; as a matter of fact, according to the simple dipole−dipole approximation, a bent structure will be characterized by a shorter interchromophoric distance, which should increase the coupling, but also by a smaller orientational factor, which, by contrast, should decrease the coupling. Hence, these two effects should largely compensate each other and a linear structure is a reasonable representation of the dyad geometry.

Different model systems representing the single chromophores (PDI, TDI) or the chromophores including one (PDI-B1, TDI-B1), two (PDI-B2, TDI-B2), or all three (PDI-B3, TDI-B3) phenyl units of the bridge were built to compute the electronic coupling between the two dyes. Such models were obtained by simply eliminating bridge atoms and then introducing hydrogens at standard bond lengths to saturate valences of the appropriate carbon atoms. We note, however, that all the three steps involved in the calculation of the electronic coupling—i.e., the calculation of the D and A transition properties and of their interaction—were performed in the cavity of the complete PDI−TDI dyad.

TD-B3LYP/6-31G(d) calculations of the transition densities and the corresponding electronic couplings were performed in vacuum and in the presence of the dielectric, which was characterized by both static and optical dielectric permittivities equal to 2.22 to mimic the polarizing effect of the poly-(methylmetacrylate) film (PMMA) environment. Additional calculations were performed in vacuum at the TD-B3LYP/6-311++G(d,p) level to check the sensibility of the results on the basis set.

In addition, possible bridge-mediated charge-transfer contributions to the coupling were explored in the presence of the environment applying the Harcourt model[45] in solution as described in ref 46. Such calculations were performed by using molecular orbitals obtained at the PCM−HF/6-31G(d) level and by considering the HOMO and LUMO orbitals localized on each chromophore. In this case, we tested several conformations by systematically changing the dihedral angle between the PDI and the TDI chromophores and its adjacent phenyl unit. The results obtained point to a negligible contribution from charge-transfer terms to the electronic coupling in the PDI−TDI dyad, and to a very small impact of the conformational motion.

All IEFPCM calculations were carried out using the cavity corresponding to the complete PDI−TDI dyad, which was constructed from radii obtained by applying the United Atom Topological Model to the atomic radii of the UFF[47] force field as implemented in the Gaussian 03 code.[48] Additional calculations were also performed by scaling these radii by constant factors 1.2 and 1.4 to check the sensitivity of our results on the precise location of the solute−solvent boundary. We found a very weak dependency of the coupling on the cavity size (changes smaller than 1 cm^{-1} were typically found by using a value 1.4 for the scaling, i.e., by using radii enlarged by 40%). All calculations were done by using a local version of Gaussian 03 adapted to perform the calculation of electronic couplings between excited states on fragments.

2c. Spectral Overlap Calculations. Absorption and emission line shapes for the PDI−TDI dyad were calculated using

$$a(\omega) = \frac{A}{\pi}\langle \mathrm{Re}\int_0^\infty \mathrm{d}t\, \exp[i(\omega - \omega_a)t - g(t)]\rangle \qquad (3)$$

$$f(\omega) = \frac{F}{\pi}\langle \mathrm{Re}\int_0^\infty \mathrm{d}t\, \exp[i(\omega - \omega_d + 2\lambda)t - g^*(t)]\rangle \qquad (4)$$

where A and F are constants, ω_a is the transition frequency for electronic state a of the acceptor, whereas ω_d is that for the donor. The angle brackets mean that the ensemble spectra are obtained by averaging the excitation energies over static disorder. The reorganization energy λ amounts to half the Stokes shift. The line shape function $g(t)$ is taken to be a sum of two overdamped Brownian oscillators ($g_{BO}(t)$) and a sum of discrete bath oscillators ($g_{DO}(t)$) where each Brownian oscillator contribution to the line shape function is defined as:

$$g_{BO}(t) = g'_{BO}(t) + ig''_{BO}(t)$$

$$g''_{BO}(t) = -(\lambda/\Lambda)[\exp(-\Lambda t) + \Lambda t - 1]$$

$$g'_{BO}(t) = (\lambda/\Lambda)\cot(\hbar\beta\Lambda/2)[\exp(-\Lambda t) + \Lambda t - 1] + \frac{4\lambda\Lambda}{\hbar\beta}\sum_{n=1}^{\infty}\frac{\exp(-\upsilon_n t) + \upsilon_n t - 1}{\upsilon_n(\upsilon_n^2 - \Lambda^2)} \qquad (5a)$$

and the discrete oscillators contribute the line shape functions according to:

$$g_{DO}(t) = \sum_j S_j[\coth(\beta\hbar\omega_j/2)(1 - \cos(\omega_j t)) + i(\sin(\omega_j t) - \omega_j t)] \qquad (5b)$$

$\beta = (k_B T)^{-1}$, k_B is the Boltzmann constant and T the temperature in Kelvin, and the Matsubara frequencies are defined as $\upsilon_n \equiv 2\pi n/(\hbar\beta)$.

Two Brownian oscillators were used to fit the single molecule line shapes satisfactorily (see Figure 4). We used the same function for both PDI and TDI. The first Brownian oscillator has a reorganization energy of 110 cm^{-1} and a modulation frequency (Λ) of 1/(50 fs). The second has a reorganization energy of 20 cm^{-1} and a modulation frequency of 1/(1 ps). We found that satisfactory fits to the spectral line shapes recorded at 1.2 K could not be achieved using a single Brownian oscillator. That is not surprising since it is well-known that a characteristic feature of condensed phase environments is the multitude of fluctuation time scales (in other words, the bath spectral density is rather complex). These fluctuations carry the same characteristic time scales at all temperatures, but their amplitude is strongly moderated by temperature, see the real part of $g_{BO}(t)$ in eq 5a. Intuitively, that is because at low temperature thermal fluctuations do not allow the systems to sample such a broad distribution of modes. The precise choice of parameters for the line shape functions cannot be obtained by fitting linear spectroscopic data, so the parameters we have used are approximate. However, since our spectral overlap calculations do not account for bath memory effects, coherences, or correlated fluctuations, possible inaccuracies in the bath representation are of no consequence. Note that the line shape models of eq 5 are appropriate at all temperatures (i.e., we have not invoked a high temperature approximation). The frequencies, ω_j, and Huang−Rhys factors, S_j, used for the discrete oscillators were determined by fitting the distinct vibrational structure in the low-temperature single molecule spectra. The results are collected in Table 1. All calculations pertain to the experimental data recorded at 1.2 K.

The spectral overlap is determined as usual as the integrated overlap of the area normalized line shape functions:[36]

$$J = \int_0^\infty \mathrm{d}\omega\, \langle a_A^{\mathrm{hom}}(\omega;\omega_a + \delta_a)\, f_D^{\mathrm{hom}}(\omega;\omega_d + \delta_d)\rangle \qquad (6)$$

TABLE 1: Frequencies, ω_j, and Huang−Rhys Factors, S_j, of the Discrete Bath Oscillators Used in the Simulation of the Low-Temperature Single Molecule Spectra from ref 39

TDI acceptor		PDI donor	
ω_j (cm^{-1})	S_j	ω_j (cm^{-1})	S_j
1286.4	0.15	1582.2	0.16
507.4	0.03	1384.9	0.17
183.1	0.07	1307.8	0.26
113.0	0.09	110.2	0.14
45.7	0.03	205.1	0.14
21.3	0.02	87.2	0.07
97.0	0.09	313.0	0.04
160.0	0.05	538.4	0.09
55.0	0.06	1059.6	0.02
76.0	0.05	260.0	0.02
		70.0	0.02

TABLE 2: Transition Dipoles (μ^T, in Debye) and Vertical Excitation Energies (E, in eV), as Computed at the TD-B3LYP/6-31G(d) Level in Vacuum and in the PMMA Matrix for the Different Models of the PDI and TDI Chromophores[a]

	vacuum		PMMA	
	E	μ^T	E	μ^T
PDI	2.44	8.88	2.33	10.08
PDI-B1	2.43	9.48	2.32	10.62
PDI-B2	2.43	9.82	2.31	10.86
PDI-B3	2.43	10.00	2.31	10.97
TDI	1.97	12.67	1.83	14.36
TDI-B1	1.96	13.29	1.82	14.87
TDI-B2	1.96	13.61	1.82	15.09
TDI-B3	1.96	13.79	1.82	15.20

[a] B1, B2, and B3 indicate that the model chromophore includes one, two or three phenyl units from the bridge, respectively.

where δ_f and δ_a are the static offsets for donor emission and acceptor absorption spectra respectively, and the angle brackets mean ensemble averaging over these offsets. The offsets are selected from normal distributions centered about a zero mean. The superscript "hom" means that each $a_A^{hom}(\omega;\omega_a + \delta_a)$ and $f_D^{hom}(\omega;\omega_d + \delta_d)$, the acceptor absorption and donor emission line shapes, denote homogeneous line shape functions normalized to unit area on a frequency scale. The Förster method assumes the following ensemble averaging

$$J \approx \int_0^\infty d\omega \langle a(\omega;\omega_a + \delta_a)\rangle\langle f(\omega;\omega_f + \delta_f)\rangle \qquad (7)$$

which is equivalent to eq 6 when one considers only a donor−acceptor pair (i.e., rather than aggregated donors or acceptors[36]).

3. Results and Discussion

To ease the analysis of the results, we have split the discussion section into three parts devoted to: (i) the excited-state properties of the PDI and TDI single chromophores; (ii) the nature and magnitude of their electronic coupling; and (iii) the calculation of the RET rates together with comparison to experiment.

3a. Single Chromophores. As a preliminary test, we analyze the performance of the IEFPCM TD-B3LYP scheme adopted here to describe the spectroscopic properties of the single chromophores. In Table 2, we report the values of the transition energies and transition dipoles obtained with the 6-31G(d) basis set for the PDI and TDI single chromophore models including none, one, two, or three phenyl units of the *p*-terphenyl bridge.

In accord with the experimental observation, the introduction of the bridge units does not substantially affect the transition energies of the PDI and TDI units (<1% change). On the other hand, the introduction of phenyl units in the model chromophores does affect the transition dipole, which increases by ∼13% (PDI) and ∼9% (TDI) in vacuum, while this effect is slightly smaller in the PMMA matrix, with increases of ∼9 and ∼6%, respectively.

TABLE 3: Screening Factors (s) and Electronic Couplings (V) Obtained from TD-B3LYP/6-31G(d) Calculations in Vacuum and in PMMA[a]

	vacuum		PMMA				
donor−acceptor	V	V_{dd}	V_s	$V_{explicit}$	V	s	V_{dd}/n^2
PDI−TDI	56.1	52.1	73.3	−42.2	31.0	0.42	30.2
PDI−TDI-B1	64.9	54.7	81.7	−46.9	34.8	0.43	31.3
PDI-B1−TDI	66.0	55.7	83.3	−47.7	35.5	0.43	31.8
PDI−TDI-B2	76.3	56.0	90.6	−51.2	39.4	0.43	31.8
PDI-B2−TDI	78.2	57.6	93.3	−52.7	40.6	0.43	32.6
PDI-B1−TDI-B1	77.6	58.4	93.8	−53.2	40.6	0.43	33.0
PDI−TDI-B3	95.1	56.7	103.7	−55.6	48.1	0.46	32.0
PDI-B1−TDI-B2	94.7	59.9	106.1	−58.1	48.0	0.45	33.5
PDI-B2−TDI-B1	95.4	60.4	107.2	−58.8	48.4	0.45	33.7
PDI-B3−TDI	97.1	58.7	107.2	−57.8	49.4	0.46	32.9

[a] The contributions, V_s and $V_{explicit}$, to the total coupling (see text) together with the PDA (point-dipole approximation) electronic couplings, V_{dd}, are also given. B1, B2, and B3 indicate that the model chromophore includes one, two or three phenyl units from the bridge, respectively. All couplings are in cm^{-1}.

The single molecule spectra at low T indicate that the most intense (0−0) transition occurs at ∼2.3 eV in PDI and ∼1.9 eV in TDI. The calculated vertical transition energies for PDI and TDI in PMMA amount to ∼2.32 and ∼1.82 eV, respectively, and are in excellent agreement with experiment. We further checked the effect of the basis set on our results. Using a split-valence triple-ζ basis set with diffuse and polarization functions (6-311++G(d,p)) leads for both chromophores to a slight decrease (by ∼0.1 eV) in the transition energies with respect to the 6-31G(d) basis set. In addition, the use of this enlarged basis set has minor effects on the magnitude of the electronic couplings (that differ by less than 1% from the 6-31G(d) values). We are therefore confident on the reliability and accuracy of the chosen level of theory to describe electronic energy transfer in the PDI−TDI dyad.

3b. Electronic Couplings. We now move to the analysis of the electronic coupling obtained for the different model chromophores. Table 3 collects the couplings obtained at the TD-B3LYP/6-31G(d) level in vacuum and in PMMA matrix, as well as the screening factors s (see section 1b) and the values estimated from the point dipole approximation, V_{dd}, obtained by using transition dipoles from the corresponding TD-B3LYP calculations. We have computed all possible pairs for the PDI and TDI model chromophores.

Interestingly, the couplings only weakly depend on the way the phenyl rings of the bridge are shared among the PDI and TDI chromophores, i.e., PDI−TDI-B1 and PDI-B1−TDI for one phenyl ring; PDI−TDI-B2, PDI-B2−TDI and PDI-B1−TDI-B1 for two phenyl rings; PDI−TDI-B3, PDI-B1−TDI-B2, PDI-B2−TDI-B1, and PDI-B3−TDI for three phenyl units yield essentially the same electronic couplings. Yet, these couplings significantly increase with the number of phenyl units in the bridge: in vacuum, a value of 56.1 cm^{-1} is obtained in absence of the bridge, while the introduction of one, two, or three phenyl units in the spacer leads to increased values of ∼65−66, ∼76−78, and ∼95−97 cm^{-1}, respectively. We note that all these couplings arise from the Coulomb term in eq 2b, while exchange and overlap terms are found to be negligible.

The origin of this bridge-mediated contribution to the coupling, very similar in vacuum and in the PMMA matrix,

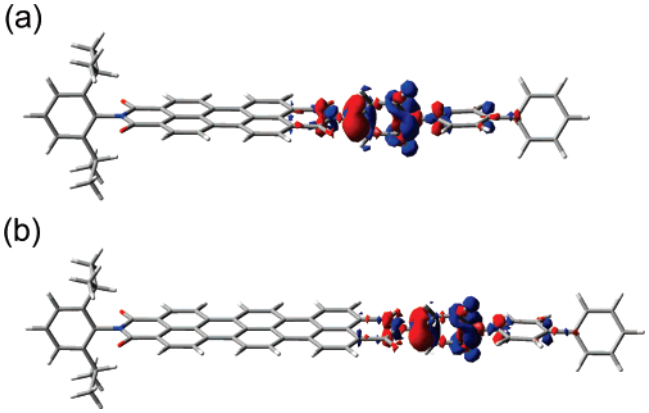

Figure 2. Graphical representation of the difference in transition density between (a) PDI-B3 and PDI and (b) TDI-B3 and TDI.

can be understood through the analysis of the transition densities obtained for the different chromophores.

In Figure 2, the difference between transition densities of PDI-B3 and PDI, and of TDI-B3 and TDI are reported.

From these pictures it appears evident that the bridge-induced changes take essentially the form of a spreading of the transition densities over the terphenyl spacer. That means that the bridge-mediated contribution to the coupling results from superexchange interactions, i.e., allowing the states of the bridge and those of the PDI(TDI) dyes to interact leads to a slight delocalization of the transition densities over the spacer, which in this case results in a net increase in the coupling between PDI and TDI. Interestingly, the addition of the first and the second phenyl units of the bridge lead to similar enhancements on the coupling (by $\sim$10 cm^{-1}), while the addition of the third phenyl unit of the bridge leads to a larger effect (by $\sim$19 and $\sim$14 cm^{-1} in vacuum and in PMMA, respectively). On that basis, we thus anticipate an even larger effect for spacers including four or more phenylene rings. In the framework of a superexchange mechanism, the amount of bridge-donor and bridge-acceptor mixing indeed increases with decreasing energy mismatch between the end-caps and the spacer (hence also with the size of the conjugated bridge).

Further insight in the nature of the interactions can be obtained by comparing the couplings computed from the transition densities to those obtained from the point dipole approximation (using a distance between chromophoric center-of-masses equal to 27.9 Å). The disagreement between the two sets of results gets worse when the number of phenyl rings included in the bridge is increased. This indicates that in the PDI − TDI model of the dyad (without the bridge) the Coulomb coupling is reasonably well described by the point dipole approximation, which underestimates the coupling by $\sim$8%). However, the introduction of the spacer induces a change of the transition densities which leads to the breakdown of the dipole−dipole approximation (underestimation of $\sim$31%). In this case, a shorter effective interchromophoric distance accounting for the delocalization of the transition densities in the spacer should be used for the dipole−dipole coupling. However, such shifted "centers" of transition density cannot be straightforwardly defined.

When accounting for the medium effects in the PMMA matrix, we predict a further increase in the Coulomb-exchange couplings, V_s, compared to the V values in vacuum for all the considered pairs. The physical origin of this effect can be traced back to the polarizing effect exerted by the PMMA matrix on the transition densities of the PDI and TDI units. In addition, the PMMA environment also adds a direct contribution on the coupling, $V_{explicit}$, which describes the interaction between the PDI and TDI transition densities mediated by the environment (see Figure 3).

This effect leads to a screening of the interaction, and can be quantified by the screening factor s introduced in Section 2b, which can be directly compared to the $s = 1/n^2$ value used in Förster theory. For the most complete models of the dyad (that consider the three phenyl units of the bridge), we find a very good agreement between the IEFPCM value of s (0.45−0.46) and that predicted from Förster theory, $s = 1/n^2 = 0.45$ (with $n = 1.49$). However, we note that this agreement is not universal, and we indeed found out recently that s is distance-dependent in a set of over 100 chromophore pairs extracted from photosynthetic antenna proteins.[33,34]

We finally estimate the electronic coupling in the real dyad as the average value obtained in PMMA for the four models considering the three phenyl units of the bridge: 48.5 cm^{-1}. By comparing this value with that obtained without the spacer, we quantify the bridge-mediated contribution to the coupling as 17.5 cm^{-1}, i.e. 36% of the total coupling. It has to be noted that the whole analysis has been done using fixed PDI−B and TDI−B dihedral angles; possible effects due to changes in these values have been checked both on the excitation energies and on the couplings. A complete scan of the dihedral angles has revealed changes of less than 1% in excitation energies and 3% in electronic couplings when these angles are varied (either in phase or with opposite phase) from 90° to 0°.

3c. RET Rates. As the first step for calculating the RET rates for the PDI−TDI dyad we simulated the representative single chromophore PDI (donor) emission and TDI (acceptor) absorption spectra at a temperature of 1.2 K as described in section 2c. The simulated spectra as well as the experimental data[39] are shown in Figure 4.

The procedure is described in Section 2 and the high-frequency vibrations, obtained by fitting the experimental data, are collected in Table 1. In addition to the homogeneous line broadening described in Section 2 (the Brownian oscillator bath model), we added a small "micro-inhomogeneous" line broadening, assumed to be a Gaussian distribution of static frequency offsets with standard deviation 6 cm^{-1}. That accounts for slow changes in the local environment around each chromophore during the bin time of the experiment, and is explained by Jang and Silbey.[49] We do not include this micro-inhomogeneous line broadening in calculations of the RET rates. It is worth re-emphasizing here that based only on fitting the linear optical spectra it is difficult to obtain the details of the line shape functions, particularly the precise time scales of the bath. The inhomogeneous contribution makes the line shapes slightly more Gaussian in shape than predicted solely by the Brownian oscillator functions.

As the bridged dyad is in PMMA, the effects of structural fluctuations are assumed to be minimal, and thus the donor−acceptor separation and orientation are held fixed. As a result, the distribution of RET time constants estimated by experiment[39] arises from the spectral overlap distribution throughout the ensemble which is caused by inhomogeneous line broadening. That is, at each site in the PMMA film the donor and acceptor experience a slightly different local environment, which adds an offset to their transition energies, and that offset is essentially static on the time scale of the experiment.[50] As usual, we assume that this distribution of static energy offsets follows a Gaussian distribution and we obtain reasonable estimates of the standard deviation of the distributions for donor and acceptor by simulating ensemble spectra (1.2 K) using a Monte Carlo sampling procedure over 8000 realizations of disorder selected

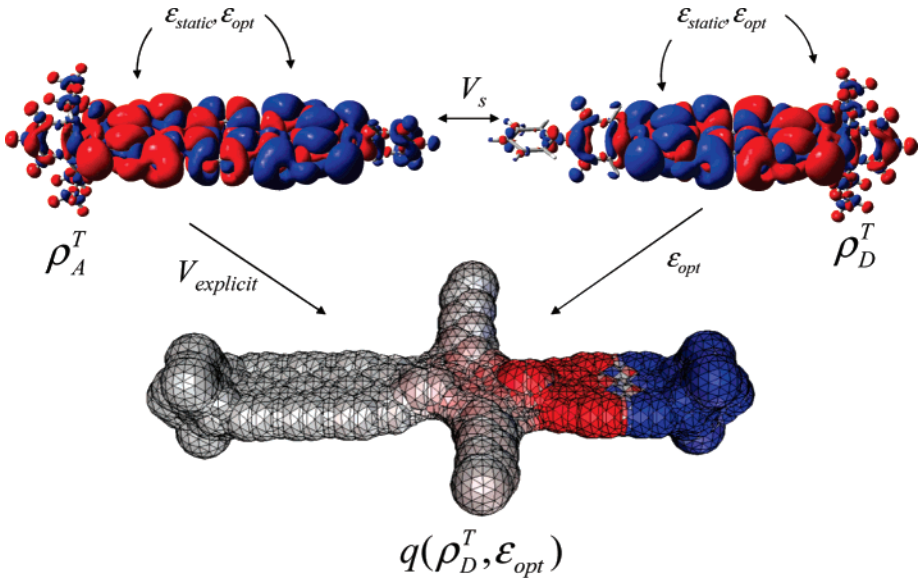

Figure 3. Graphical representation of the transition densities obtained for the PDI-B2 (ρ_D^T) and TDI-B1 (ρ_A^T) model chromophores as well as the IEFPCM reaction potential (represented on the cavity surface) generated by the PMMA matrix in response to the PDI-B2 transition, $q(\rho_D^T, \epsilon_{opt})$. The contributions to the RET coupling in the TD−DFT IEFPCM model are defined as the interaction between ρ_D^T and ρ_A^T for V_s, and between $q(\rho_D^T, \epsilon_{opt})$ and ρ_A^T for the environment-mediated term $V_{explicit}$.

from the distribution. Those results are plotted in Figure 5, where we have used standard deviations of 300 and 350 cm^{-1} for the inhomogeneous contribution to the line broadening of TDI and PDI, respectively.

In complex condensed phase environments like liquids or polymer films the length scale over which the bath fluctuations are correlated ought to be quite short. Therefore we assume for the dyads that the static offset of the donor and acceptor transitions are uncorrelated in each dyad, in accord to what is observed experimentally.[39] Using the calculated electronic coupling of 48.5 cm^{-1} we calculated the RET time constant in 8000 dyads randomly selected from the ensemble. It was found that a few thousand dyads were sufficient to obtain the statistics of the ensemble. Simulations based on just a few hundred samples did not seem to give sufficient information on the distribution to extract quantitative results. The resulting distribution of RET time constants is plotted in Figure 6 and the mean of the distribution is found to be 8 ps. These results appear to be in reasonable agreement with experiment.[39] In these calculations, the distribution of RET rates is determined solely by the spectral overlap distribution, which is calculated using the ensemble averaging and eq 6. We find $J = 6.625 \times 10^{-5}$ cm.

It is notable that our calculations of the RET time constant distribution (and hence the spectral overlap distribution) are consistent with the experimental observations reported by Métivier, et al.[39] The experimental results might suggest a somewhat faster RET rate, depending upon how effectively the 84 measurements sampled represent the ensemble. That would, in turn, suggest that there may be some correlation between donor and acceptor static offsets or that our calculated electronic couplings are underestimated. Another possible origin to the mismatch between measured and calculated rates is the presence of vibrational modes that couple simultaneously to the PDI and TDI units. These have been shown to yield a renormalized phonon reorganization energy for RET compared to optical

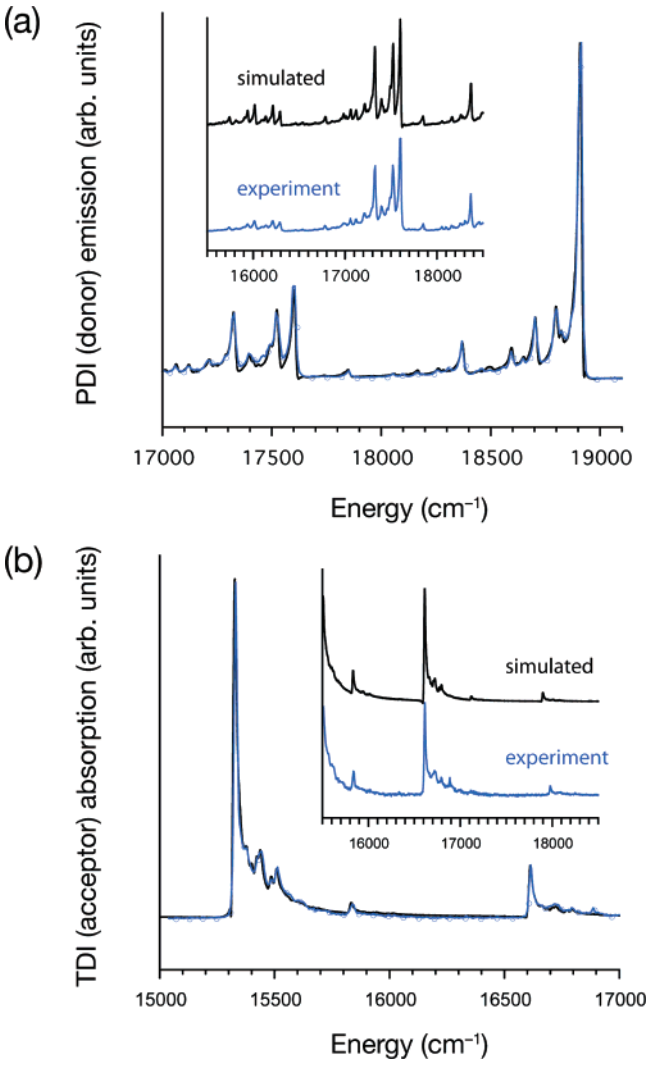

Figure 4. Simulated spectra (black lines) compared to experimental data for single chromophores at 1.2 K[39] (blue lines with symbols). (a) PDI donor emission spectrum. (b) TDI acceptor absorption spectrum.

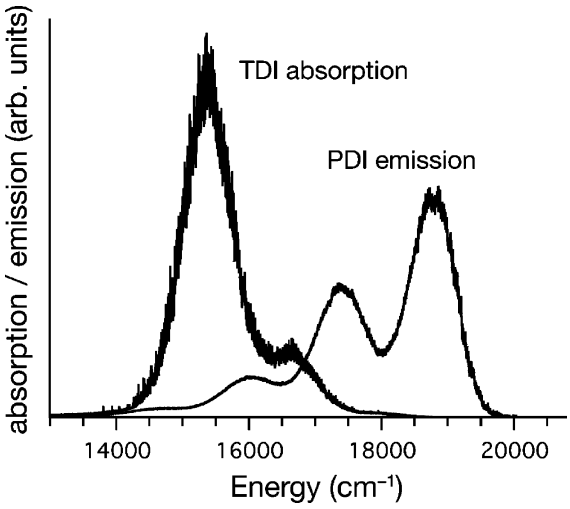

Figure 5. Ensemble TDI absorption and PDI emission spectra calculated by assuming a static inhomogeneous broadening for each ensemble of chromophores of 300 and 350 cm^{-1}, respectively. These inhomogeneous line widths are estimated by comparing the spectra to ensemble room-temperature data. Changing these values within reasonable limits did not affect the conclusions of our RET calculations.

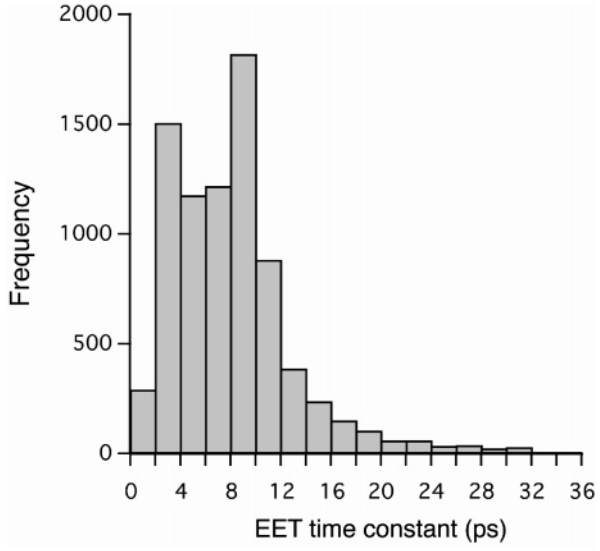

Figure 6. Histogram(s) of RET time constants obtained through calculations of 8000 individual donor−acceptor pairs taken randomly from the ensemble under the assumption that the inhomogeneous line broadening for the donor and acceptor is uncorrelated. The mean RET time constant is 8 ps. This distribution can be compared to the experimental results reported in Figure 4a of ref 39. Our results show a longer mean RET time (by a factor of ∼2) and a more pronounced tail to longer RET times.

excitation over the donor and acceptor such that the transfer rate can no longer be factorized into donor emission and acceptor absorption lineshapes.[51] It is also worth mentioning the discrepancy between our calculated spectral overlap distribution and that reported in ref 39, which is clearly very broad and does not follow a normal distribution. We therefore conclude that experiment matches the calculation much more closely than was initially realized. Nonetheless, the dipole−dipole approximation for the electronic coupling is significantly different from that obtained from a more accurate calculation. We conclude that the precise role of the spacer in mediating this electronic coupling arises from superexchange interactions, which lead to a slight delocalization of the transition densities over the terphenyl spacer, such an effect inducing a ∼56% increase in the coupling and thus to a 2−3 fold increase in the rate. This bridge-induced effect leads to a breakdown of the dipole−dipole approximation, which otherwise works reasonably well for the separated PDI and TDI dyes but misses ca. one-third of the coupling in the bridged dyad.

4. Conclusions

In the present work, we have assessed the applicability of the Förster model to predict the dynamics of electronic energy transfer in a model donor−acceptor dyad at low temperature: A terphenyl-bridged PDI−TDI dyad embedded in a PMMA film. To this end, we have quantitatively accounted for all salient ingredients involved in the Förster rate: electronic coupling, spectral overlap, and the screening of the environment.

Electronic couplings were obtained as the interaction between the transition densities of the PDI and TDI chromophores using a quantum-mechanical approach based on time-dependent density functional theory (at the TD-B3LYP level). The effect of the PMMA environment was included self-consistently both on the transition densities and on their interaction through the IEFPCM continuum model. In addition, we analyzed in detail the role of the bridge on the electronic interaction by considering the p-terphenyl spacer in the calculations. We find that superexchange interactions associated with the bridge, and apparent as a slight delocalization of the PDI(TDI) transition densities over the spacer, result in an increase by 56% of the coupling in the dyad. This effect leads to a breakdown of the dipole−dipole approximation used in Förster theory, which underestimates (by ca. one-third) the coupling in the presence of the spacer, but does well (with less than 10% error) for bare PDI and TDI at the same separation.

On the other hand, we found an excellent agreement between the Förster screening factor $1/n^2$ and the screening factor obtained from IEFPCM-TDDFT calculations, which is obtained by considering a molecular-shaped cavity (enclosing the PDI−TDI dyad) inside the PMMA dielectric environment. We note however that this result is not universal, as the precise value of the screening depends on the particular shape, distance, and orientation of the chromophore pair under consideration and can deviate significantly from the Förster estimate.[33,34]

The spectral overlap was determined as the integrated overlap of the area normalized line shape functions of the donor emission and the acceptor absorption, which were accurately simulated by comparison to experimental single molecule spectra at 1.2 K. The distribution of spectral overlap throughout the ensemble was estimated by assuming an uncorrelated inhomogeneous line broadening for the donor and acceptor, both following a Gaussian distribution, and by randomly selecting 8000 dyads from the ensemble. Combining this distribution of spectral overlap with the calculated electronic coupling of 48.5 cm^{-1} we obtained a distribution of RET times with mean value of 8 ps. It is remarkable that our distribution of RET times (and hence the spectral overlap distribution) is consistent with the experimental observations reported by Métivier, et al.,[39] the latter pointing to a somewhat faster measured RET rate. We conclude that for this dyad the main limitation of the Förster rate expression is the dipole−dipole approximation used to estimate the coupling, which is incapable of describing the large increase in the coupling induced by the presence of the bridge due to superexchange interactions.

Acknowledgment. We thank Thomas Basché for fruitful discussions and for providing us the measured single-molecule absorption spectrum of TDI in the dyad and emission spectrum

of the free PDI dye. C.C. and B.M. acknowledge the financial support of the Italian "Ministero dell'Università e Ricerca" (PRIN 2005). The work in Mons has been partly supported by the Belgian Federal Government "Interuniversity Attraction Pole in Supramolecular Chemistry and Catalysis, PAI 5/3", the Belgian National Fund for Scientific Research (FNRS/FRFC), the European STREP project MODECOM (NMP−CT-2006-016434), and the European IP project NAIMO (NMP4-CT-2004-500355). D.B. is a research director of FNRS. G.D.S. acknowledges the support of an E.W.R. Steacie Memorial Fellowship from the Natural Sciences and Engineering Research Council of Canada.

Note Added in Proof. After the submission of our manuscript, we note that similar conclusions on the role of the bridge to the electronic coupling in the PDI-TDI dyad have been reported by Fückel et al. (Fückel, B.; Köhn, A.; Harding, M. E.; Diezemann, G.; Hinze, G.; Basché, T.; Gauss, J. To be published in the *J. Chem. Phys.*

References and Notes

(1) Scholes, G. D. *Annu. Rev. Phys. Chem.* **2003**, *54*, 57.
(2) Fleming, G. R.; Scholes, G. D. *Nature* **2004**, *431*, 256.
(3) Sundström, V.; Pullerits, T.; van Grondelle, R. *J. Phys. Chem. B* **1999**, *103*, 2327.
(4) van Amerongen, H.; Valkunas, L.; van Grondelle, R. *Photosynthetic Excitons*; World Scientific Publishers: Singapore, 2000.
(5) Jares-Erijman, E. A.; Jovin, T. M. *Nat. Biotech.* **2003**, *21*, 1387.
(6) Lippincott-Schwartz, J.; Snapp, E.; Kenworthy, A. *Nat. Rev. Mol. Cell Biol.* **2001**, *2*, 444.
(7) Weiss, S. *Nat. Struct. Biol.* **2000**, *7*, 724.
(8) List, E. W. J.; Holzer, L.; Tasch, S.; Leising, G.; Scherf, U.; Müllen, K.; Catellani, M.; Luzzati, S. *Solid State Comm.* **1999**, *109*, 455.
(9) Lee, J.-I.; Kang, I.-N.; Hwang, D.-H.; Shim, H.-K.; Jeoung, S. C.; Kim, D. *Chem. Mater.* **1996**, *8*, 1925.
(10) Wang, H.-L.; McBranch, D. W.; Klimov, V. I.; Helgeson, R.; Wudl, F. *Chem. Phys. Lett.* **1999**, *315*, 173.
(11) Halls, J. J. M.; Walsh, C. A.; Greenham, N. C.; Marseglia, E. A.; Friend, R. H.; Moratti, S. C.; Holmes, A. B. *Nature* **1995**, *376*, 498.
(12) Sariciftci, N. S.; Smilowitz, L.; Heeger, A. J.; Wudl, F. *Science* **1992**, *258*, 1474.
(13) Yu, G.; Gao, J.; Hummelen, J. C.; Wudl, F.; Heeger, A. J. *Science* **1995**, *270*, 1789.
(14) Chen, L.; McBranch, D. W.; Wang, H.-L.; Helgeson, R.; Wudl, F.; Whitten, D. G. *Proc. Natl. Acad. Sci. U.S.A.* **1999**, *96*, 12287.
(15) Jones, R. M.; Lu, L.; Helgeson, R.; Bergstedt, T. S.; McBranch, D. W.; Whitten, D. G. *Proc. Natl. Acad. Sci. U.S.A.* **2001**, *98*, 14769.
(16) Swager, T. M.; Wosnick, J. H. *MRS Bull.* **2002**, *27*, 446.
(17) Wang, D.; Gong, X.; Heeger, P. S.; Rininsland, F.; Bazan, G. C.; Heeger, A. J. *Proc. Natl. Acad. Sci. U.S.A.* **2002**, *99*, 49.
(18) Stork, M.; Gaylord, B. S.; Heeger, A. J.; Bazan, G. C. *Adv. Mater.* **2002**, *14*, 361.
(19) Zhou, Q.; Swager, T. M. *J. Am. Chem. Soc.* **1995**, *117*, 12593.
(20) McQuade, D. T.; Pullen, A. E.; Swager, T. M. *Chem. Rev.* **2000**, *100*, 2537.
(21) McQuade, D. T.; Hegedus, A. H.; Swager, T. M. *J. Am. Chem. Soc.* **2000**, *122*, 12389.
(22) Zigmantas, D.; Read, E. L.; Manèal, T.; Brixner, T.; Gardiner, A. T.; Cogdell, R. J.; Fleming, G. R. *Proc. Natl. Acad. Sci. U.S.A.* **2006**, *103*, 12672.
(23) Hennebicq, E.; Pourtois, G.; Scholes, G. D.; Herz, L. M.; Russell, D. M.; Silva, C.; Setayesh, S.; Grimsdale, A. C.; Mullen, K.; Bredas, J.-L.; Beljonne, D. *J. Am. Chem. Soc.* **2005**, *127*, 4744.
(24) Förster, T. *Ann. Phys. (Berlin)* **1948**, *2*, 55.
(25) Krueger, B. P.; Scholes, G. D.; Fleming, G. R. *J. Phys. Chem. B* **1998**, *102*, 5378.
(26) Beljonne, D.; Cornil, J.; Silbey, R.; Millie, P.; Bredas, J. L. *J. Chem. Phys.* **2000**, *112*, 4749.
(27) Beljonne, D.; Pourtois, G.; Silva, C.; Hennebicq, E.; Herz, L. M.; Friend, R. H.; Scholes, G. D.; Setayesh, S.; Müllen, K.; Brédas, J. L. *Proc. Natl. Acad. Sci. U.S.A.* **2002**, *99*, 10982.
(28) Wong, K. F.; Bagchi, B.; Rossky, P. J. *J. Phys. Chem. A* **2004**, *108*, 5752.
(29) Iozzi, M. F.; Mennucci, B.; Tomasi, J.; Cammi, R. *J. Chem. Phys.* **2004**, *120*, 7029.
(30) Beenken, W. J. D.; Pullerits, T. *J. Chem. Phys.* **2004**, *120*, 2490.
(31) Wiesenhofer, H.; Beljonne, D.; Scholes, G. D.; Hennebicq, E.; Brédas, J. L.; Zojer, E. *Adv. Funct. Mater.* **2005**, *15*, 155.
(32) Madjet, M. E.; Abdurahman, A.; Renger, T. *J. Phys. Chem. B* **2006**, *110*, 17268.
(33) Scholes, G. D.; Curutchet, C.; Mennucci, B.; Cammi, R.; Tomasi, J. *J. Phys. Chem. B* **2007**, *111*, 6978.
(34) Curutchet, C.; Scholes, G. D.; Mennucci, B.; Cammi, R. *J. Phys. Chem. B* **2007**, *111*, 13253.
(35) (a) Pullerits, T.; Freiberg, A. *Chem. Phys.* **1991**, *149*, 409. (b) Pullerits, T.; Hess, S.; Herek, J. L.; Sundstrom, V. *J. Phys. Chem. B* **1997**, *101*, 10560.
(36) Scholes, G. D.; Jordanides, X. J.; Fleming, G. R. *J. Phys. Chem. B* **2001**, *105*, 1640.
(37) Becker, K.; Lupton, J. M. *J. Am. Chem. Soc.* **2006**, *128*, 6468.
(38) Becker, K.; Lupton, J. M.; Feldmann, J.; Setayesh, S.; Grimsdale, A. C.; Mullen, K. *J. Am. Chem. Soc.* **2006**, *128*, 680.
(39) Métivier, R.; Nolde, F.; Müllen, K.; Basché, T. *Phys. Rev. Lett.* **2007**, *98*, 47802.
(40) (a) Cancès, E.; Mennucci, B. *J. Math. Chem.* **1998**, *23*, 309. (b) Cancès, E.; Mennucci, B.; Tomasi, J. *J. Chem. Phys.* **1997**, *107*, 3032. (c) Mennucci, B.; Cancès, E.; Tomasi, J. *J. Phys. Chem. B* **1997**, *101*, 10506.
(41) (a) Miertus, S.; Scrocco, E.; Tomasi, J. *Chem. Phys.* **1981**, *55*, 117. (b) Cammi, R.; Tomasi, J. *J. Comput. Chem.* **1995**, *16*, 1449.
(42) Tomasi, J.; Mennucci, B.; Cammi, R. *Chem. Rev.* **2005**, *105*, 2999.
(43) Curutchet, C.; Mennucci, B. *J. Am. Chem. Soc.* **2005**, *127*, 16733.
(44) Fückel, B.; Hinze, G.; Diezemann, G.; Nolde, F.; Müllen, K.; Gauss, J.; Baschè, T. *J. Chem. Phys.* **2006**, *125*, 144903.
(45) Harcourt, R. D.; Scholes, G. D.; Ghiggino, K. P. *J. Chem. Phys.* **1994**, *101*, 10521.
(46) Russo, V.; Curutchet, C.; Mennucci, B. *J. Phys. Chem. B* **2007**, *111*, 853.
(47) Rappé, A. K.; Casewit, C. J.; Colwell, K. S.; Goddard, W. A., III; Skiff, W. M. *J. Am. Chem. Soc.* **1992**, *114*, 10024.
(48) Frisch, M. J.; Trucks, G. W.; Schlegel, H. B.; Scuseria, G. E.; Robb, M. A.; Cheeseman, J. R.; Montgomery, J. A., Jr.; Vreven, T.; Kudin, K. N.; Burant, J. C.; Millam, J. M.; Iyengar, S. S.; Tomasi, J.; Barone, V.; Mennucci, B.; Cossi, M.; Scalmani, G.; Rega, N.; Petersson, G. A.; Nakatsuji, H.; Hada, M.; Ehara, M.; Toyota, K.; Fukuda, R.; Hasegawa, J.; Ishida, M.; Nakajima, T.; Honda, Y.; Kitao, O.; Nakai, H.; Klene, M.; Li, X.; Knox, J. E.; Hratchian, H. P.; Cross, J. B.; Bakken, V.; Adamo, C.; Jaramillo, J.; Gomperts, R.; Stratmann, R. E.; Yazyev, O.; Austin, A. J.; Cammi, R.; Pomelli, C.; Ochterski, J. W.; Ayala, P. Y.; Morokuma, K.; Voth, G. A.; Salvador, P.; Dannenberg, J. J.; Zakrzewski, V. G.; Dapprich, S.; Daniels, A. D.; Strain, M. C.; Farkas, O.; Malick, D. K.; Rabuck, A. D.; Raghavachari, K.; Foresman, J. B.; Ortiz, J. V.; Cui, Q.; Baboul, A. G.; Clifford, S.; Cioslowski, J.; Stefanov, B. B.; Liu, G.; Liashenko, A.; Piskorz, P.; Komaromi, I.; Martin, R. L.; Fox, D. J.; Keith, T.; Al-Laham, M. A.; Peng, C. Y.; Nanayakkara, A.; Challacombe, M.; Gill, P. M. W.; Johnson, B.; Chen, W.; Wong, M. W.; Gonzalez, C.; Pople, J. A. *Gaussian 03*, revision B.05; Gaussian, Inc.: Wallingford, CT, 2004.
(49) Jang, S.; Silbey, R. J. *J. Chem. Phys.* **2003**, *118*, 9312.
(50) Fleming, G. R.; Passino, S. A.; Nagasawa, Y. *Phil. Trans. R. Soc. London A* **1998**, *356*, 389.
(51) Hennebicq, E.; Beljonne, D.; Silbey, R. J. submitted.